THE JOURNAL OF PHYSICAL CHEMISTRY A
A JOURNAL OF THE AMERICAN CHEMICAL SOCIETY

pubs.acs.org/JPCA

Article

Photodissociation Dynamics of Astrophysically Relevant Propyl Derivatives (C_3H_7X; X = CN, OH, HCO) at 157 nm Exploiting an Ultracompact Velocity Map Imaging Spectrometer: The (Iso)Propyl Channel

Published as part of The Journal of Physical Chemistry virtual special issue "Combustion in a Sustainable World: From Molecules to Processes".

Dababrata Paul, Zhenghai Yang, Shane J. Goettl, Aaron M. Thomas, Chao He, Arthur G. Suits, David H. Parker, and Ralf I. Kaiser*

Cite This: *J. Phys. Chem. A* 2022, 126, 5768−5775

Read Online

ACCESS | Metrics & More | Article Recommendations

ABSTRACT: The photodissociation dynamics of astrophysically relevant propyl derivatives (C_3H_7X; X = CN, OH, HCO) at 157 nm exploiting an ultracompact velocity map imaging (UVMIS) setup has been reported. The successful operation of UVMIS allowed the exploration of the 157 nm photodissociation of six (iso)propyl systems—*n*/*i*-propyl cyanide (C_3H_7CN), *n*/*i*-propyl alcohol (C_3H_7OH), and (iso)butanal (C_3H_7CHO)—to explore the C_3H_7 loss channel. The distinct center-of-mass translational energy distributions for the *i*-C_3H_7X (X= CN, OH, HCO) could be explained through preferential excitation of the low frequency C−H bending modes of the formyl moiety compared to the higher frequency stretching of the cyano and hydroxy moieties. Although the ionization energy of the *n*-C_3H_7 radical exceeds the energy of a 157 nm photon, $C_3H_7^+$ was observed in the *n*-C_3H_7X (X = CN, OH, HCO) systems as a result of photoionization of vibrationally "hot" *n*-C_3H_7 fragments, photoionization of *i*-C_3H_7 after a hydrogen shift in vibrationally "hot" *n*-C_3H_7 radicals, and/or two-photon ionization. Our experiments reveal that at least the isopropyl radical (*i*-C_3H_7) and possibly the normal propyl radical (*n*-C_3H_7) should be present in the interstellar medium and hence searched for by radio telescopes.

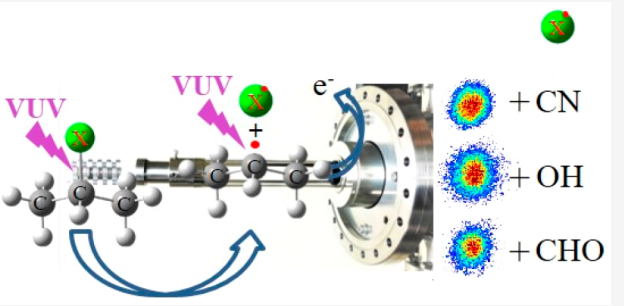

1. INTRODUCTION

Complex organic molecules (COMs)—per astronomical definition organic molecules containing several atoms of carbon, hydrogen, oxygen, and nitrogen such as aldehydes (HCOR) [1], alcohols (ROH) [2], and nitriles (RCN) [3] with R representing an alkyl group—are ubiquitous in the interstellar medium (ISM).[1] An understanding of the abiotic formation pathways of COMs is of vital importance to the laboratory astrophysics and astronomy communities. The synthesis of COMs has been linked to the processing of low temperature (10 K) ice-coated interstellar grains though ionizing radiation, such as galactic cosmic rays (GCRs) and the internal ultraviolet (UV) photons in cold molecular clouds, such as the Taurus Molecular Cloud 1 (TMC-1).[2−4] The densest parts of these clouds undergo gravitational collapse ultimately resulting in star forming regions with temperatures of up to 300 K. This temperature increase results in a (partial) sublimation of the COMs into the gas phase, where they can be detected by radio telescopes.[5] Since the transition from a cold molecular cloud to star forming regions critically depends on the molecular composition, it is vital to elucidate the fundamental processes of how COMs are not only formed, but also photolytically destroyed in those environments.[6,7] In this context, a fundamental knowledge of the formation and photolysis of structural isomers such as functionalized propyl (*n*-C_3H_7) and isopropyl (*i*-C_3H_7) derivatives of complex organics is of vital significance since these pairs of structural isomers are recognized as tracers of the physical and chemical conditions of interstellar environments and to test chemical

Received: June 26, 2022
Revised: August 3, 2022
Published: August 22, 2022

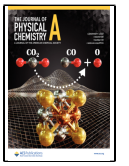

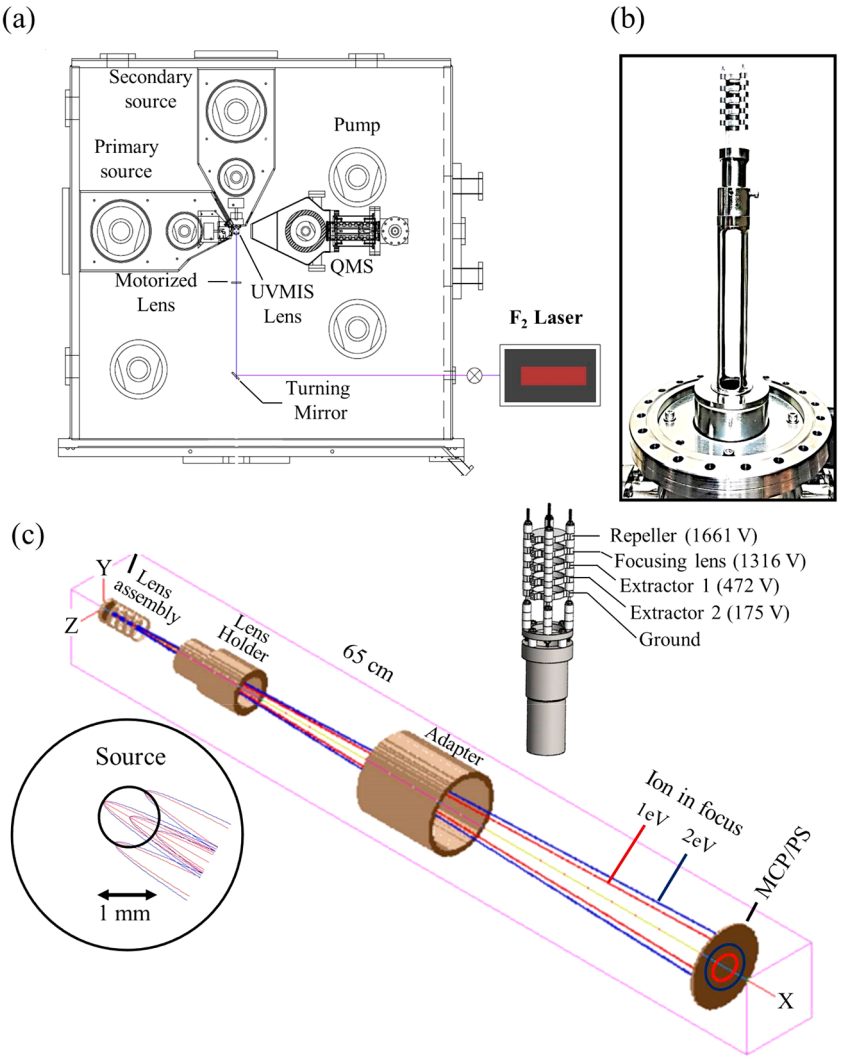

Figure 1. Layout of the ultracompact velocity map imaging system (UVMIS) incorporated within a universal crossed molecular beam machine (a). The fluorine (F_2) laser is connected with the main chamber through a gate valve. QMS: Triply differentially pumped quadrupole mass spectrometer; primary and secondary molecular beam source. The motorized focusing lens and turning mirror are positioned in the vacuum to allow the 157 nm beam alignment. The photograph of the UVMIS lens assembly is shown in panel b. The optimum geometrical parameters of the lenses by SIMION simulation are compiled in (c). Ions of mass-to-charge (m/z) of 43 ($C_3H_7^+$) with kinetic energies of 1 and 2 eV fly onto the microchannel plate/phosphor screen (MCP/PS) detector. The lens assembly is an open cylindrical type with the outer diameter of 20 mm and thickness of 4.65 mm. The ion spot in the origin of the ionizing laser and molecular beam interaction is displayed in lower left corner. Five points of ion (red solid lines, 1 eV; blue solid lines, 2 eV) with ±90° ejection angles in a 1 mm spherical source are considered to predict the trajectories. The voltage set for velocity mapping condition is shown on top right corner. The simulation was performed with the SIMION (version 8, Scientific Instrument Services) program package.

models of molecular clouds and star forming regions through astrochemical modeling.

In star forming regions, such as Sagittarius B2 (SgrB2), fully saturated nitriles (X = CN), alcohols (X = OH), and aldehydes (X = HCO) $CH_3(CH_2)_nX$ (n = 0−1) carrying the methyl and ethyl group have been observed astronomically over the past decades.[8−13] Considering the rising complexity, nitriles and alcohols carrying the propyl (n-C_3H_7) and isopropyl (i-C_3H_7) groups, that is, propylnitrile (n-C_3H_7CN)[14] and isopropylnitrile (i-C_3H_7CN),[15] along with propanol (n-C_3H_7OH)[16] and isopropanol (i-C_3H_7OH),[16] were detected only recently in SgrB2 with searches for alcohols guided by recent laboratory studies of exposing ices of carbon monoxide (^{13}CO) and methane ($^{13}CD_4$) toward proxies of galactic cosmic rays (GCR).[4] As of now, neither butanal (n-C_3H_7CHO) nor isobutanal (i-C_3H_7CHO) has been observed astronomically toward any source, although laboratory simulation experiments of ^{13}CO−$^{13}CD_4$ ices interacting with GCR proxies predict their presence in Sgr(B2).[4]

Once sublimed from the icy grains into the gas phase in star forming regions, the intense photon flux can photoionize and photodissociate these gas phase molecules.[17,18] For instance, photodissociation of methanol (CH_3OH) generates methoxy (CH_3O), hydroxymethyl (CH_2OH), and methyl (CH_3) radicals via O−H, C−H, and C−O bond rupture, respectively.[18] At 193 nm, the methoxy (CH_3O) radical represents the dominant product,[19] whereas hydroxymethyl (CH_2OH) and methyl (CH_3) radicals are formed predominantly at 157 nm.[20] Photodissociation of ethanol (CH_3CH_2OH) and n-propyl alcohol ($CH_3CH_2CH_2OH$) follows a similar pattern, such as the generation of the ethoxy (CH_3CH_2O) photofragment.[21,22] The photodissociation of aldehydes (RCHO, R =

https://doi.org/10.1021/acs.jpca.2c04430
J. Phys. Chem. A 2022, 126, 5768−5775

$CH_3(CH_2)_n$; n = 0−2) was also explored, and C−H and C−C bond rupture were determined to be the major decomposition pathways leading to RCO and HCO radicals, respectively.[23−26] Secondary dissociation of these fragments via, for example, atomic hydrogen loss leading to $(CH_2)_{n+1}CO$ (n = 0−2) and carbon monoxide (CO), respectively, strongly depend on the internal energy redistribution prior to bond breaking with the yield of the secondary products increasing as the photon energy rises. In contrast to aforementioned systems, photodissociation of nitriles (R-CN, R = $CH_3(CH_2)_n$; n = 0−2) is less diverse and exhibits predominantly the carbon−carbon cleavage to the cyano radical (CN) plus the alkyl radical fragment (R).[27,28] The quantum yield decreases with the length of the alkyl chain due to intramolecular vibrational energy redistribution (IVR).

Although ample photodissociation studies have been conducted for the $CH_3(CH_2)_nX$ (X = OH, CN, HCO; n = 0−1) systems as compiled above, photodissociation of the corresponding (iso)propyl systems have escaped thorough experimental studies in particular at higher photon energies (157 nm).[22,25−27,29,30] In this work, we explore the photodissociation dynamics of propyl (n-C_3H_7) and isopropyl (i-C_3H_7) organics carrying a cyano, hydroxyl, and formyl functional group, that is, n/i-propyl cyanide (C_3H_7CN), n/i-propyl alcohol (C_3H_7OH), and (iso)butanal (C_3H_7CHO), in a molecular beam at 157 nm leading to (iso)propyl radicals (C_3H_7) exploiting an ultracompact velocity map imaging spectrometer (UVMIS) incorporated into a molecular beams machine. The UVMIS design is first tested and benchmarked through one known system of the photodissociation of 2,3-dimethylpentane (C_7H_{16}) at 157 nm followed by photoionization of the propyl radical fragment with a second 157 nm photon.[31] The successful operation of the UVMIS allowed the exploration of the 157 nm single photon dissociation of six (iso)propyl systems—n/i-propyl cyanide (C_3H_7CN), n/i-propyl alcohol (C_3H_7OH), and (iso)butanal (C_3H_7CHO)—as a function of laser pulse energy thus providing insights into the inherent photodissociation dynamics and isomerization processes on the C_3H_7 potential energy surface (PES).

2. EXPERIMENT

The UVMIS is designed exploiting the multielectrode concept with lens dimensions of 20 mm × 20 mm × 35 mm and embodied in a universal crossed molecular beam machine (Figure 1).[32] Multielectrodes incorporating an open cylindrical geometry offer an advanced control of the shape of the electric field in the spectrometer.[33,34] The five electrodes, that is, repeller, focusing lens, extractor 1, extractor 2, and ground, are stacked and separated by 3.5 mm between the repeller and focusing and 2.5 mm between the remaining electrodes through aluminum oxide insulators resulting in an overall length of 35 mm of the multielectrode system. Voltages were optimized to remove any blurring of finite source size (Figure 1). The voltage ratio between the focusing lens and the repeller was 0.80; voltages of the successive electrodes gradually decrease to zero.

For each photodissociation experiment, a pulsed supersonic molecular beam of C_3H_7X (X = CN, OH, HCO) seeded in helium carrier gas (99.9999%, Airgas) at a backing pressure of 1,013 Torr was generated via a pulsed, piezo-crystal driven valve at 10 Hz and 80 μs pulse width.[35] Chemicals were purchased from Sigma-Aldrich with the purity i-propyl cyanide (C_3H_7CN) 99.6%, n-propyl cyanide (C_3H_7CN) ≥ 99%, i-propyl alcohol (C_3H_7OH) 99.9%, n-propyl alcohol (C_3H_7OH) ≥ 99.9%, butanal (C_3H_7CHO) ≥ 99.5%, and isobutanal (C_3H_7CHO) ≥ 99%. The molecular beam was skimmed by a skimmer of 1 mm diameter and entered the main chamber, where it intersected the 157 nm laser pulse perpendicularly. The velocity and speed ratio of each molecular beam was determined with a triply differentially pumped quadruple mass spectrometer (QMS, Extrel, QC 150, 2.1 MHz oscillator) and Daly type ion counter[35] operated in the time-of-flight (TOF) mode after electron impact ionization (80 eV, 2 mA) of the neutral molecules (Table 1). The delay between the laser pulse and the molecular beam as compiled in Table 1 was set at a position so that the laser pulse interacted the very early rising edge of molecular beam to eliminate photodissociation of clusters.

Table 1. Velocity (v), Speed Ratio, and Delay Parameters of Each Molecular System Are Presented[a]

compounds	v (m s^{-1})	speed ratio	L_{TOF} (mm)	$t_{arrival}$ (μs)
2,3-dimethylpentane	1523	6.8	45	29.54
n/i-propyl cyanide	1631	7.2		27.59
n/i-propyl alcohol	1369	3.4		32.87
(iso)butanal	1144	5.9		39.33

[a]Pulse valve has 200 μs internal delay.

A fluorine (F_2) laser (GAM Ex-10) was used to generate a 157 nm laser pulse with the latter introduced into the main chamber through a double sided 16 KF gate valve. The 157 nm pulse was reflected at a turning mirror (Acton Optics & Coatings) and then focused by a 210 mm lens (Acton Optics & Coatings) after passing a 1 mm aperture to interact with the molecular beam. Laser energy was 0.62 mJ per pulse at a repetition rate of 10 Hz. Note that the 157 nm photons were used to first photodissociate the organic molecule and then to photoionize the resulting C_3H_7 radicals formed. The resultant $C_3H_7^+$ ion cloud was accelerated and focused by the UVMIS system onto a position sensitive detector composed of a dual-chevron microchannel plate (MCP) and a phosphor screen. The front plate of the MCP was set to zero volts; the back plate was biased to 1.0 kV then pulsed for 150 ns at +2.3 kV at the arrival time of the $C_3H_7^+$ ions. Upon impact on the MCP front plate, the signal was thereby amplified, and an image was generated on the phosphor screen. The visible image on the phosphor screen was captured by a charge couple device (CCD) camera (IDS, UI-2230SE-M-GL) placed outside the vacuum chamber viewing the phosphor through a glass window. 15 000 laser shots were averaged by the NuAcq software to construct each image.[36] Background ion counts were removed from the images by subtracting a background image collected without the molecular beam under otherwise identical experimental conditions. This setup was also exploited for the calibration experiment of the 157 nm photodissociation of 2,3-dimethylpentane (C_7H_{16}, ≥99%) seeded at a fraction of 0.5% in helium carrier gas. 10 000 laser shots were averaged in the same procedure mentioned above to construct the image. FINA software was used to treat the raw images, and for conversion to translational energy distribution.[37]

3. RESULTS AND DISCUSSION

3.1. Reference Experiment. To experimentally test the capabilities of the UVMIS design, we first performed a test

https://doi.org/10.1021/acs.jpca.2c04430
J. Phys. Chem. A 2022, 126, 5768−5775

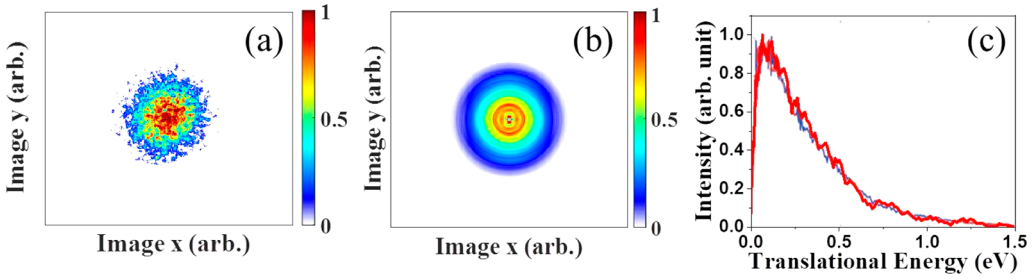

Figure 2. Raw (a) and reconstructed (b) images of $C_3H_7^+$ (m/z = 43) from the photodissociation of 2,3-dimethylpentane (C_7H_{16}) at 157 nm. In panel c, the normalized translational energy distribution, red solid line, derived from panel b was adapted together with the translational energy distribution profile, blue solid line, reported in ref 31.

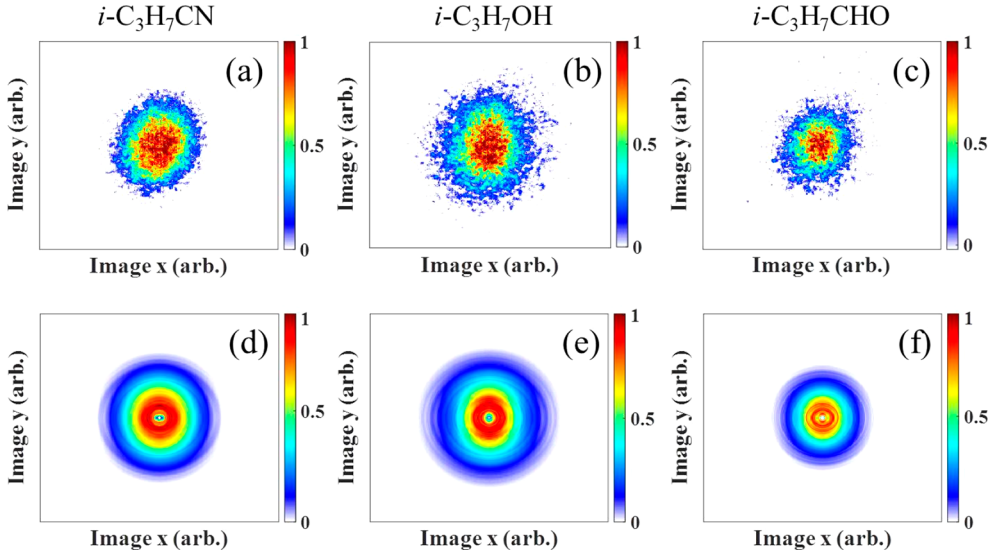

Figure 3. Raw (upper) and reconstructed (lower) images of $C_3H_7^+$ (m/z = 43) from the photodissociation of i-C_3H_7X (X = CN, OH, HCO) at 157 nm. The images a and d are for isobutyronitrile (i-C_3H_7CN), b and e for isopropanol (i-C_3H_7OH), and c and f for isobutyraldehyde (i-C_3H_7CHO), respectively.

experiment on the photodissociation of 2,3-dimethylpentane (C_7H_{16}) at 157 nm to compare to prior work. The goal of the photodissociation experiment was to examine and to eliminate any distortions of the image; further, because of the compact nature of the imaging setup, voltages and the parameters of the pulsed valve were optimized to eliminate any discharges due to potentially excessive gas loads in the photoionization region. Preliminary experiments optimize the experimental parameters at likely kinetic energy releases we wish to measure. For example, for the high kinetic energy measurement, the repeller voltage must be set at a level so that the detector covers the whole image. After setting the repeller voltage, the focusing voltage should be set at a position to get the best resolution for desired kinetic energy release, as the best focusing shifted to lower or higher in energy with increasing or decreasing the focusing voltage. Thus, the energy calibration is necessary prior to perform any new experiments. To study the photodissociation of propyl derivatives (C_3H_7X; X = CN, OH, HCO), the UVMIS was calibrated with the known kinetic energy distribution of propyl radical (C_3H_7) in the photodissociation of 2,3-dimethylpentane (C_7H_{16}) under velocity mapping conditions with voltage settings of the repeller (1661 V), focusing lens (1316 V), the extractor 1 (472 V), extractor 2 (175 V), and ground. The raw image of the $C_3H_7^+$ ions is symmetric and agrees well with the reference image.[31]

The raw image, reconstructed image, and translational energy distribution of $C_3H_7^+$(m/z = 43) stemming from the photolysis of 2,3-dimethylpentane (C_7H_{16}) at 157 nm are shown in Figure 2. The two-dimensional (2D) raw image is the projection of a Newton sphere formed in the interaction region. The total translational energy distribution is obtained from the velocity distribution by $E_T = \frac{1}{2}\frac{m_{DF}}{m_{CF}}(m_{DF} + m_{CF})v_{DF}^2$ at the center-of-mass through a sharp slice by using FINA software, where m_{DF} and m_{CF} represent the detected mass and cofragment mass, respectively. A narrow slice was reconstructed by removing the out-of-plane elements using radial basis functions. The translational energy distribution of the ion is treated separately with the coproduct and adapted together with the reference translational energy distribution for comparison in Figure 2c.[31] The experimentally obtained translational energy distribution collected here is identical with the literature distribution and allows us to set value for conversion from the velocity profile in pixel unit to kinetic energy release of the fragments.

3.2. Photodissociation of Propyl Derivatives (C_3H_7X; X = CN, OH, CHO). To investigate the photodissociation dynamics of propyl derivatives (C_3H_7X; X = CN, OH, HCO), the raw and reconstructed images of $C_3H_7^+$ (m/z = 43) resulting from the photolysis of i-C_3H_7X (X = CN, OH, HCO) at 157 nm are shown in Figure 3. The total translational energy

https://doi.org/10.1021/acs.jpca.2c04430
J. Phys. Chem. A 2022, 126, 5768−5775

distributions of each photodissociation channel is obtained from the velocity distribution with the calibration factor determined in the photodissociation of 2,3-dimethylpentane (C_7H_{16}) at 157 nm, and compiled in Figure 4.

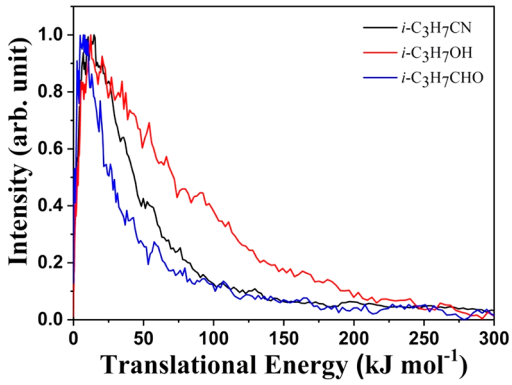

Figure 4. Center-of-mass translational energy distributions of the photodissociation of i-C_3H_7X (X= CN, OH, HCO) at 157 nm. The relative signal intensity of each system was obtained by integrating three-dimensional velocity distributions of their corresponding images in Figure 3.

The translational energy distributions of the $C_3H_7^+$ ions are quite distinct for isobutyronitrile, isopropanol, and isobutyraldehyde. The translational energy distribution of the propyl radical ion ($C_3H_7^+$) for the i-C_3H_7OH system is the broadest and reveals an average translational energy release of about 47.7 kJ mol^{-1}. For the isobutyronitrile and isobutyraldehyde systems, the average kinetic energy release extend to 34.2 and 29.8 kJ mol^{-1}; the isobutyraldehyde system reveals on average the lowest energy channeling into the translational degrees of freedom. Further, all center-of-mass translational energy distributions reveal a distribution maximum at about 10 kJ mol^{-1} suggesting a rather loose exit transition state with a simple carbon−carbon bond rupture. The aforementioned differences in kinetic energy release resulting from three molecular systems of i-C_3H_7X (X = CN, OH, HCO) may suggest a decrease in channeling of the total available energy into the internal (rovibrational) degrees of freedom from the formyl (HCO) via the cyano (CN) to the hydroxyl (OH) radical during the photodissociation process. In other words, the high frequency modes of the OH and CN stretching of 3738 and 2069 cm^{-1} compared to the three normal modes of the formyl (C−H stretching, 2434 cm^{-1}; C−H bending, 1081 cm^{-1}; CO stretching, 1868 cm^{-1}) would preferentially result in vibration quanta into the low frequency C−H bending mode of the formyl moiety, which translates into a lower fraction of energy into the translational degrees of freedom as observed experimentally (Figure 4). Thus, i-C_3H_7CN and i-C_3H_7OH have very similar translational energy partitioning (13.1% and 13.2%), while it is only 7.2% for i-C_3H_7CHO. These values indicate that the radical fragments are highly rovibrationally excited. The formyl (HCO) and hydroxyl (OH) channels may suggest ground state dissociation, but the cyano channels could be associated with both ground state and excited state decay.

The available energy of each molecular system has been calculated by the energy balance via $E_{aval} = E_{h\nu} - D_0 + E_{int}$, where $E_{h\nu}$, D_0, and E_{int} represent the photon energy, the dissociation energy of C−X, and the internal energy of the parent molecules, respectively. The C−X bond dissociation energies of each system are determined based on the enthalpies of formation of each species at standard conditions from National Institute of Standards and Technology (NIST). The internal energies of the parent molecules are assumed to be zero as they are expanded under supersonic molecular beam conditions. The detail energy partitioning of each system are displayed in Scheme 1.

Finally, we explored the photodissociation of the corresponding isomers, n-C_3H_7X (X = CN, OH, HCO). The raw (upper) and reconstructed (lower) images, as well as center-of-mass translational energy resulting from the photolysis of n-C_3H_7X (X = CN, OH, CHO) at 157 nm are shown in Figures 5 and 6, respectively. The total translational energy distributions for these three molecular systems are nearly

Scheme 1. Energy Level Diagram for the Photodissociation of i-C_3H_7X/n-C_3H_7X (X = CN, OH, CHO) at 157 nm[a]

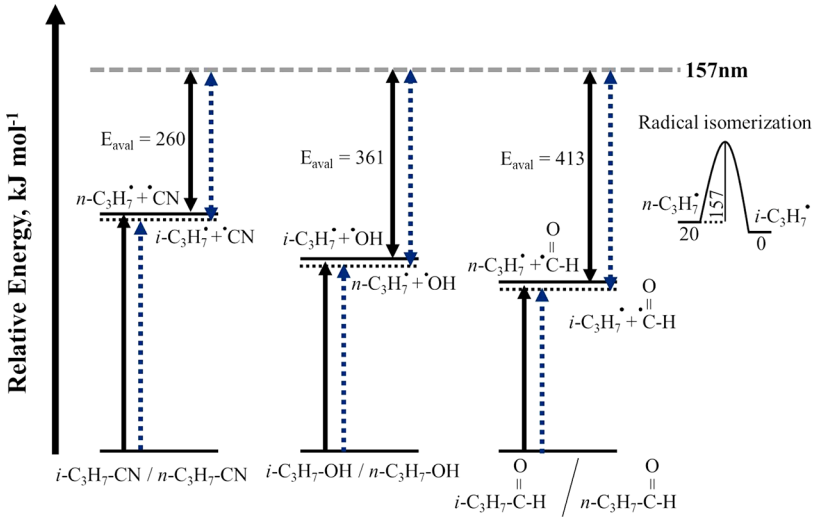

[a]The solid and dotted lines represent for the i-C_3H_7X and n-C_3H_7X molecular systems, respectively. The relative energies shown are enumerated based on the enthalpies of formation of each species at standard conditions from NIST. Radical isomerization of n-C_3H_7 to i-C_3H_7 with a barrier 157 kJ mol^{-1} is shown on top right corner and open in each system.

https://doi.org/10.1021/acs.jpca.2c04430
J. Phys. Chem. A 2022, 126, 5768−5775

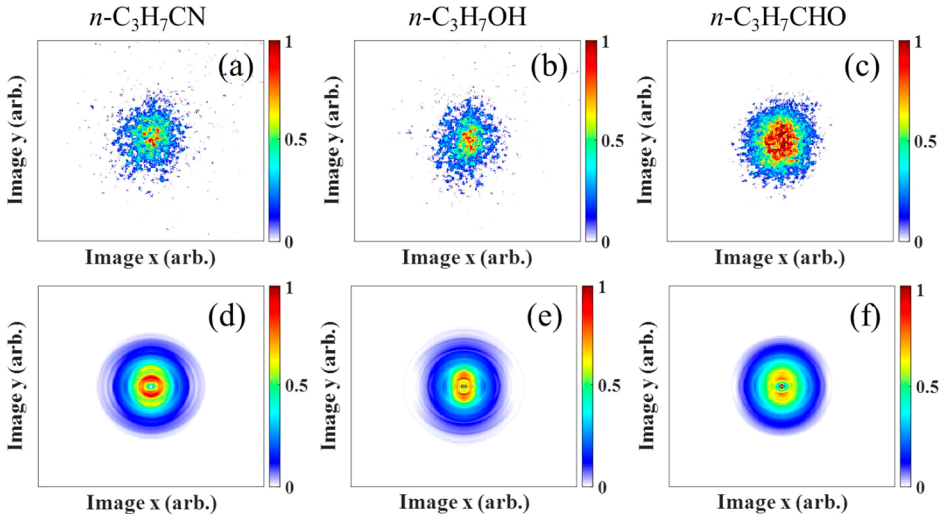

Figure 5. Raw (upper) and reconstructed (lower) images of $C_3H_7^+$ (m/z = 43) from the photodissociation of n-C_3H_7X (X = CN, OH, HCO) at 157 nm. The images a and d are for butyronitrile (n-C_3H_7CN), b and e for 1-propanol (n-C_3H_7OH), and c and f for butyraldehyde (n-C_3H_7CHO), respectively.

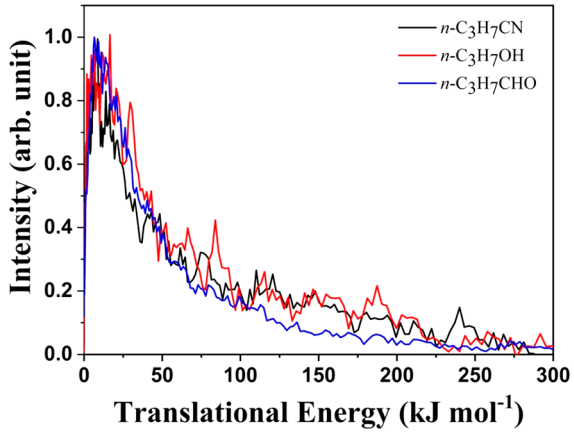

Figure 6. Center-of-mass translational energy distributions of the photodissociation of n-C_3H_7X (X = CN, OH, HCO) at 157 nm. The relative signal intensity of each system was obtained by integrating three-dimensional velocity distributions of their corresponding images in Figure 5.

identical. The contribution of available energy to the translation of these systems declines from 11.1% for n-C_3H_7CN via 8.3% for n-C_3H_7OH to 7.2% for n-C_3H_7CHO. Note that the translational energy distribution profiles of n-C_3H_7X are narrower compared to the translational energy distribution profiles of their isomers, i-C_3H_7X. This energy reduction, 25 kJ mol^{-1}, is not surprising as the energy difference is very close to the energy difference, 20 kJ mol^{-1}, between the formation of two isomers of propyl radical (C_3H_7).[38]

It is important to note that the adiabatic ionization energy of the n-C_3H_7 radical of 8.09 eV (780 kJ mol^{-1}) is higher than the energy of the 157 nm photon of 7.89 eV (762 kJ mol^{-1}) by 18 kJ mol^{-1}. Therefore, rovibrationally cold n-C_3H_7 radicals should not be photoionized by a 157 nm photon. However, this simple picture fails to account for the internal energy of the n-C_3H_7 radical fragment born in the photodissociation process. This internal energy can result in the photoionization of vibrationally "hot" n-C_3H_7 radicals. Alternatively, each system has sufficient excess energy to allow the n-C_3H_7 radical to isomerize into the i-C_3H_7 radical via hydrogen shift (Scheme 1), which then can be photoionized (IE = 7.37 eV). The barrier height for n-C_3H_7 to i-C_3H_7 transition via [1,2]-H shift was calculated to be 157 kJ mol^{-1}.[38]

Considering the energy level diagram, the available energies 260, 361, and 413 kJ mol^{-1} for n-C_3H_7CN, n-C_3H_7OH, and n-C_3H_7CHO, respectively, are sufficient to open up the isomerization channel. The detection of ion signal at m/z = 43 suggests that either vibrationally "hot" n-C_3H_7 radicals are photoionized or that n-C_3H_7 radicals isomerize to i-C_3H_7 radicals prior to their photoionization. Note that, in case of the n-C_3H_7 systems, the first 157 nm photon reaches 97% the way to ionization. Therefore, an overlap with Rydberg states exists, and ionization of n-C_3H_7 could be the result of multiphoton ionization.

4. CONCLUSION

We reported the photodissociation of astrophysically relevant iso- and normal-propyl derivatives (C_3H_7X; X = CN, OH, HCO) at 157 nm exploiting the new design of a compact electrostatic lens system for velocity map imaging (UVMIS). The UVMIS is constructed in a space effective manner with lens dimensions of 20 mm × 20 mm × 35 mm that fit well to existing universal crossed molecular beam machines. The open cylindrical lens configuration has a unique advantage over the closed cylindrical lens in terms of elimination of charging effect. The performance of the UVMIS is tested by studying the photodissociation of 2,3-dimethylpentane (C_7H_{16}) at 157 nm. The successful operation of the UVMIS allowed the exploration of the 157 nm single photon dissociation of six (iso)propyl systems—n/i-propyl cyanide (C_3H_7CN), n/i-propyl alcohol (C_3H_7OH), and (iso)butanal (C_3H_7CHO)—as a function of laser pulse energy and to explore the C_3H_7 loss channel. The distinct center-of-mass translational energy distributions for the i-C_3H_7X (X = CN, OH, HCO) could be explained through preferential excitation of the low frequency C−H bending modes of the formyl moiety compared to the higher frequency stretching of the cyano and hydroxy moieties, respectively. Most important, although the ionization energy of the n-C_3H_7 radical is higher than the energy of a 157 nm photon, $C_3H_7^+$ was observed in the n-

https://doi.org/10.1021/acs.jpca.2c04430
J. Phys. Chem. A 2022, 126, 5768−5775

C_3H_7X (X = CN, OH, HCO) systems as a result of photoionization of vibrationally "hot" n-C_3H_7 fragments, photoionization of i-C_3H_7 after a hydrogen shift in vibrationally n-C_3H_7 radicals, and multiphoton ionization. Finally, our experiments reveal that at least the isopropyl radical (i-C_3H_7) and possibly the normal propyl radical (n-C_3H_7) should be present in the interstellar medium and, hence, searched for by radio telescopes.

AUTHOR INFORMATION

Corresponding Author

Ralf I. Kaiser − *Department of Chemistry, University of Hawai'i at Manoa, Honolulu, Hawaii 96822, United States;* orcid.org/0000-0002-7233-7206; Email: ralfk@hawaii.edu

Authors

Dababrata Paul − *Department of Chemistry, University of Hawai'i at Manoa, Honolulu, Hawaii 96822, United States*

Zhenghai Yang − *Department of Chemistry, University of Hawai'i at Manoa, Honolulu, Hawaii 96822, United States*

Shane J. Goettl − *Department of Chemistry, University of Hawai'i at Manoa, Honolulu, Hawaii 96822, United States*

Aaron M. Thomas − *Department of Chemistry, University of Hawai'i at Manoa, Honolulu, Hawaii 96822, United States;* orcid.org/0000-0001-8540-9523

Chao He − *Department of Chemistry, University of Hawai'i at Manoa, Honolulu, Hawaii 96822, United States*

Arthur G. Suits − *Department of Chemistry, University of Missouri, Columbia, Missouri 65211, United States;* orcid.org/0000-0001-5405-8361

David H. Parker − *Department of Laser Physics, Institute for Molecules and Materials, Radboud University, Nijmegen 6500, The Netherlands;* orcid.org/0000-0003-0297-168X

Complete contact information is available at: https://pubs.acs.org/10.1021/acs.jpca.2c04430

Notes

The authors declare no competing financial interest.

ACKNOWLEDGMENTS

This work was supported by the U.S. Department of Energy, Basic Energy Sciences (Grant No. DE-FG02-03ER15411), to the University of Hawaii at Manoa. The authors wish to thank Prof. Chul Hoon Kim (Korea University, Republic of Korea), and Chatura Perera (Suits Group, University of Missouri, USA) for their help in image analysis process.

REFERENCES

(1) Herbst, E.; van Dishoeck, E. F. Complex organic interstellar molecules. *Annu. Rev. Astron. Astrophys.* **2009**, *47*, 427−480.

(2) Kwan, J.; Valdes, F. Spiral gravitational potentials and the mass growth of molecular clouds. *Astrophys. J.* **1983**, *271*, 604−610.

(3) Soma, T.; Sakai, N.; Watanabe, Y.; Yamamoto, S. Complex organic molecules in Taurus Molecular Cloud-1. *Astrophys. J.* **2018**, *854*, 116.

(4) Turner, A. M.; Kaiser, R. I. Exploiting photoionization reflectron Time-of-Flight mass spectrometry to explore molecular mass growth processes to complex organic molecules in interstellar and solar system ice analogs. *Acc. Chem. Res.* **2020**, *53*, 2791−2805.

(5) Lattelais, M.; Bertin, M.; Mokrane, H.; Romanzin, C.; Michaut, X.; Jeseck, P.; Fillion, J. H.; Chaabouni, H.; Congiu, E.; Dulieu, F.; Baouche, S.; Lemaire, J. L.; Pauzat, F.; Pilmé, J.; Minot, C.; Ellinger, Y. Differential adsorption of complex organic molecules isomers at interstellar ice surfaces. *Astron. Astrophys.* **2011**, *532*, A12.

(6) Oberg, K. I.; Öberg, K. I. Photochemistry and astrochemistry: Photochemical pathways to interstellar complex organic molecules. *Chem. Rev.* **2016**, *116*, 9631−9663.

(7) Desai, R. T.; Coates, A. J.; Wellbrock, A.; Vuitton, V.; Crary, F. J.; González-Caniulef, D.; Shebanits, O.; Jones, G. H.; Lewis, G. R.; Waite, J. H.; Cordiner, M.; Taylor, S. A.; Kataria, D. O.; Wahlund, J. E.; Edberg, N. J. T.; Sittler, E. C. Carbon chain anions and the growth of complex organic molecules in titan's ionosphere. *Astrophys. J.* **2017**, *844*, L18.

(8) Ball, J. A.; Gottlieb, C. A.; Lilley, A. E.; Radford, H. E. Detection of methyl alcohol in sagittarius. *Astrophys. J.* **1970**, *162*, L203−L210.

(9) Solomon, P. M.; Jefferts, K. B.; Penzias, A. A.; Wilson, R. W. Detection of millimeter emission lines from interstellar methyl cyanide. *Astrophys. J.* **1971**, *168*, L107−L110.

(10) Gottlieb, C. A. Detection of acetaldehyde in sagittarius. *Mol. Galactic Environ., Proc. Symp.* **1973**, 181−186.

(11) Zuckerman, B.; Turner, B. E.; Johnson, D. R.; Lovas, F. J.; Fourikis, N.; Palmer, P.; Morris, M.; Lilley, A. E.; Ball, J. A.; Clark, F. O. Detection of interstellar trans-ethyl alcohol. *Astrophys. J.* **1975**, *196*, L99−L102.

(12) Johnson, D. R.; Lovas, F. J.; Gottlieb, C. A.; Gottlieb, E. W.; Litvak, M. M.; Thaddeus, P.; Guelin, M. Detection of interstellar ethyl cyanide. *Astrophys. J.* **1977**, *218*, 370−376.

(13) Hollis, J. M.; Jewell, P. R.; Lovas, F. J.; Remijan, A.; Møllendal, H. Green bank telescope detection of new interstellar aldehydes: Propenal and propanal. *Astrophys. J.* **2004**, *610*, L21−L24.

(14) Belloche, A.; Garrod, R. T.; Müller, H. S. P.; Menten, K. M.; Comito, C.; Schilke, P. Increased complexity in interstellar chemistry: detection and chemical modeling of ethyl formate and n -propyl cyanide in Sagittarius B2(N). *Astron. astrophys.* **2009**, *499*, 215−232.

(15) Belloche, A.; Garrod, R. T.; Müller, H. S. P.; Menten, K. M. Detection of a branched alkyl molecule in the interstellar medium: iso-propyl cyanide. *Science.* **2014**, *345*, 1584−1587.

(16) Abplanalp, M. J.; Góbi, S.; Bergantini, A.; Turner, A. M.; Kaiser, R. I. On the synthesis of chocolate flavonoids (propanols, butanals) in the interstellar medium. *Chemphyschem.* **2018**, *19*, 556−560.

(17) Pilling, S.; Santos, A. C. F.; Boechat-Roberty, H. M. Photodissociation of organic molecules in star-forming regions. *Astron. astrophys.* **2006**, *449*, 1289−1296.

(18) Pilling, S.; Neves, R.; Santos, A. C. F.; Boechat-Roberty, H. M. Photodissociation of organic molecules in star-forming regions. *Astron. astrophys.* **2007**, *464*, 393−398.

(19) Harich, S.; Lin, J. J.; Lee, Y. T.; Yang, X. Photodissociation dynamics of methanol at 157 nm. *J. Phys. Chem. A* **1999**, *103*, 10324−10332.

(20) Chen, Z.; Eppink, A. T. J. B.; Jiang, B.; Groenenboom, G. C.; Yang, X.; Parker, D. H. Product pair correlation in CH_3OH photodissociation at 157 nm: the OH + CH_3 channel. *Phys. Chem. Chem. Phys.* **2011**, *13*, 2350−2355.

(21) Xu, K.; Amaral, G.; Zhang, J. Photodissociation dynamics of ethanol at 193.3 nm: The H-atom channel and ethoxy vibrational distribution. *J. Chem. Phys.* **1999**, *111*, 6271−6282.

(22) Zhou, W.; Yuan, Y.; Zhang, J. Photodissociation dynamics of 1-propanol and 2-propanol at 193.3 nm. *J. Chem. Phys.* **2003**, *119*, 7179−7187.

(23) Terentis, A. C.; Hepburn, J. W.; Knepp, P. T.; Kable, S. H. Radical channel photodissociation dynamics of aliphatic aldehydes: the nascent state distribution of the HCO photoproduct. *Fiber Optic and Laser Sensors and Applications* **1995**, *2548*, 328−339.

(24) Zhu, L.; Cronin, T.; Narang, A. Wavelength-dependent photolysis of i-pentanal and t-pentanal from 280 to 330 nm. *J. Phys. Chem. A* **1999**, *103*, 7248−7253.

(25) Chen, Y.; Zhu, L.; Francisco, J. S. Wavelength-dependent photolysis of n -butyraldehyde and i -butyraldehyde in the 280−330 nm region. *J. Phys. Chem. A* **2002**, *106*, 7755−7763.

(26) Zhu, L.; Tang, Y.; Chen, Y.; Cronin, T. Wavelength-dependent photolysis of C_3-C_7 aldehydes in the 280−330 nm Region. *Spectrosc. Lett.* **2009**, *42*, 467−478.
(27) Kanda, K.; Nagata, T.; Ibuki, T. Photodissociation of some simple nitriles in the extreme vacuum ultraviolet region. *Chem. Phys.* **1999**, *243*, 89−96.
(28) Moriyama, M.; Tsutsui, Y.; Honma, K. Vacuum ultraviolet photodissociation dynamics of acetonitrile. *J. Chem. Phys.* **1998**, *108*, 6215−6221.
(29) Ross, P. L.; Van Bramer, S. E.; Johnston, M. V. Ultraviolet photodissociation of gas-phase alcohols, amines, and nitroalkanes. *Appl. Spectrosc.* **1996**, *50*, 608−613.
(30) Harrison, A. W.; Kable, S. H. Photodissociation dynamics of propanal and isobutanal: The Norrish Type I pathway. *J. Chem. Phys.* **2018**, *148*, 164308.
(31) Silva, R.; Gichuhi, W. K.; Doyle, M. B.; Winney, A. H.; Suits, A. G. Photodissociation of heptane isomers and relative ionization efficiencies of butyl and propyl radicals at 157 nm. *Phys. Chem. Chem. Phys.* **2009**, *11*, 4777−4781.
(32) Wilson, A. V.; Parker, D. S. N.; Zhang, F.; Kaiser, R. I. Crossed beam study of the atom-radical reaction of ground state carbon atoms ($C(^3P)$) with the vinyl radical ($C_2H_3(X_2A')$). *Phys. Chem. Chem. Phys.* **2012**, *14*, 477−481.
(33) Kling, N. G.; Paul, D.; Gura, A.; Laurent, G.; De, S.; Li, H.; Wang, Z.; Ahn, B.; Kim, C. H.; Kim, T. K.; Litvinyuk, I. V.; Cocke, C. L.; Ben-Itzhak, I.; Kim, D.; Kling, M. F. Thick-lens velocity-map imaging spectrometer with high resolution for high-energy charged particles. *J. Instrum.* **2014**, *9*, P05005.
(34) Sakkoula, E.; van Oorschot, B. G. M.; Parker, D. H. A compact electrostatic lens for velocity map imaging experiments. *Mol. Phys.* **2022**, *120*, e1910357.
(35) Gu, X. B.; Guo, Y.; Chan, H.; Kawamura, E.; Kaiser, R. I. Design and characteristics of a high-precision chopper wheel motor driver. *Rev. Sci. Instrum.* **2005**, *76*, 116103.
(36) Li, W.; Chambreau, S. D.; Lahankar, S. A.; Suits, A. G. Megapixel ion imaging with standard video. *Rev. Sci. Instrum.* **2005**, *76*, 063106.
(37) Thompson, J. O. F.; Amarasinghe, C.; Foley, C. D.; Suits, A. G. Finite slice analysis (FINA)—A general reconstruction method for velocity mapped and time-sliced ion imaging. *J. Chem. Phys.* **2017**, *147*, 013913.
(38) Noller, B.; Fischer, I. Photodissociation dynamics of the 2-propyl radical, C_3H_7. *J. Chem. Phys.* **2007**, *126*, 144302.

https://doi.org/10.1021/acs.jpca.2c04430
J. Phys. Chem. A 2022, 126, 5768−5775